Design and Analysis of Joint Torque Sensor for Safe Human-Robotic Collaboration

Muhammad Bilal and Sajid Iqbal
Department of Mechatronics and Control Engineering,
University of Engineering and Technology Lahore-54890, Pakistan
mbilal103@outlook.com, sajid.iqbal@uet.edu.pk

Muhammad Nadeem Akram
Mechanical, Automotive, and Materials Engineering Department
University of Windsor, Windsor, Ontario, Canada
Akram113@uwindsor.ca

Abstract

This study aims to investigate the protection and consistency during the physical human-robot collaboration to avoid serious injury. A low-cost torque sensor design is proposed to detect and measure the collision between the robot and human operator. The proposed perforated spoke type structure shifted the high-stresses location and modified the dispersal of the stresses. Moreover, the sensor response to the dynamic load and sensitivity is improved. The optimal parameters are selected based on the finite element analysis. A series of simulations were performed to validate the performance of the proposed torque sensor. The results show that the proposed design provides better performance compared to a non-perforated spoke type torque sensor.

Keywords: Torque sensor, perforated spoke structure, human-robotic collaboration.

1.0 Introduction

With the advent of the Information Age, the robots have been utilized in multiple domains that demand collaboration between the robot and humans (Dimeas et al., 2018; Choi et al., 2011) wherein the dependability of the robot and safety should be ensured former. Therefore, an interaction between the human and a robot should be established in a real- time process (Haddadin et al.,2017). Numerous sensor-less based methods have been used to detect the robot's collisions. By approximating the location of the robot, the collision can be detected from the controller information (Han et al., 2018). Nevertheless, the above method is not adequate for collision detection between the human and the robot in unfamiliar environments.

Using the electric current of each rotary actuator or the energy of the robot (Lee et al., 2015; Chen et al., 2018), the collision can be approximated by utilizing the friction model and the dynamic model of the robot. The disadvantage of using the robot model for estimation is the inaccurate model (Baroon et al., 2015). Sensor-based techniques have been extensively studied for collision detection. Vision-based sensors can be utilized to avoid the impact before the collision (Mohammad et al., 2017). The disadvantages of the vision-based sensors are visionary issues as well as the manipulation cost are too high. The sensitive sensor can measure the impacts at multiple configurations of the robot (Kim et al., 2015). However, due to wiring complexity and its capability to suppress intervention is inferior.

(a) Non-perforated spoke type structure (b) Perforated spoke type structure.

Figure 1: Spoke type joint torque sensor.

Use of a multiple-axes force/torque sensor on the robot's end effector is an additional solution (Wang et al., 2017), but it is not enough sensitive to detect the impacts that happen far from the robot's end-effector. The uni-axial torque sensor based on the data-driven technique has recently earned interest. Normally, a uni-axial torque sensor is attached to each joint of the manipulator (Park et al., 2013). It can detect the collisions on each part of the robot arm and enhance the detection's performance. The torque sensor is placed at the outer of the gear head yielding the friction quantities in the equation of motion.

To obtain a collision detection with the uni-axial torque sensor, it is required to develop the high-performance torque sensor with a smart architecture integrated shape, highly sensitive nature, and easy integration on the robot's joint (Choi et al., 2012).Torque sensors for the robot collision detection can be classified into three multiple subgroups based on the collision's recognition principle, namely optical, capacitive based and strain gauge, respectively. The optical- based torque sensor (Mai et al., 2017; Palli and Pirozzi, 2013; Mai et al., 2018) performs the torque manipulation by developing the relationship between the torque load and the deviation in the optical direction.

For the given applied torque, the capacitive based torque sensor can measure the load by variation in the capacitance (Madni et al., 2007; Lee et al., 2016; Choi et al., 2015). Using a capacitive based torque sensor, the advantages are quick dynamic varying response, light structure, and contact-less manipulation. Nevertheless, its precision is restricted due to thick shape employed into the manipulator's joints. To obtain the torque signal, the strain gauges-based torque sensor uses the strain gauges to translate small stresses into voltages (Park et al., 2014; Sun et al., 2015; Kashiri et al., 2017). Based on the strain gauges placement, the strain gauges-based torque sensor is further classified into three subgroups. One of the strain gauges types is adhesive on the exterior of a rod-shaped arrangement at 45° and 135° on the axial track (Muftah et al., 2013).

Adhesive type torque sensor is usually used along with slips ring to ensure signal processing for dynamic torque measurement. In case of second type, the torque sensor consists of pasting the strain gauges on the shear surface of an elastic support (Missinne et al., 2015). The advantage of this type of a sensor has a sealed structure and its signal manipulation unit can be encapsulated within the sensor assembly. Due to high stress occurring near spokes end, it is difficult to paste strain gauges. The third type of a torque sensor consists of pasting the strain gauges on the exterior of an elastic support (Lee et al., 2014). This type of a joint torque sensor is recommended due to high sensitivity but needs to overcome its drawbacks. This research aims to develop a common torque sensor for light duty robots for collision detection.

During the physical human robot interaction (p-HRI), the sensor must have fast response and excellent sensitivity. To encapsulate with joint assembly, the sensor must have compact structure. In this article, a new type of torque sensor has been developed and optimized on the basis of the third type of strain gauges.

2.0 Design of Torque Sensor Structure

The collision detection requirements are discussed herein, and then the design specifications are presented consequently. Afterward, the design of the sensor structure and a modified structure of the elastic spoke structure are presented.

A. Sensor Requirements

In this section, the design procedure and an optimization procedure is presented to develop a one-axis torque sensor for a light robot with a payload of 5 *kg*. To integrate with the robot's joint, the sensor dimensions must be compact. The torque sensor in the form of a hollow cylindrical shape having external and internal diameters are 78 *mm* and 10 *mm,* respectively. The sensor width is set to 14 *mm* for improved encapsulation. For a normal light service robot, its weight is normally about 20 *kg*, e.g., the UR5 robots have weight about 18.4 kg, and the KUKA LBR IIWA robots have weight 22 *kg* with a 7 *kg* payload. After the intermediate joint, the collective weight of the joints and links is comparatively low as approximately about 10 *kg*. Normally, the displacement between the intermediate joint and the end-effector is 300 *mm*. For the given payload of 5 *kg*, the capability of the sensor can be calculated as follows.

$$10kg \times 10N/kg \times 0.15m + 5kg \times 10N/kg \times 0.3m = 30Nm$$

For safety precautions, it is recommended that the contact force must not be exceeding than 10 N (Suita et al., 1995). To obtain reliable robot collision detection, the torque sensor must be able to measure a minimum interaction force of 10N. The collision location may not be always at the end- effector of the manipulator. Considering, the

minimum distance of collision from the robot's joint is 10 mm, the sensor resolution can be calculated as 10 mm × 10 N = 0.1 Nm. To determine the response frequency, a collision usually occurs within 4 to 10 ms (Yamada et al., 1997). During the collision, it is required that the robot system must detect a contact force equal to or less than 1 ms. Hence, the response frequency of the joint sensor is kept constant to 1kHz. Table 1 summarizes the associated design specifications of the joint torque sensor

Table 1: Design Specification

Parameters	Values
Size	Φ78×ϕ10×H14 mm
Capacity	30 Nm
Overload	250%F.S
Resolution	0.1 Nm
Response frequency	1 kHz

B. Torque Sensor Construction Scheme

The perforated spoke joint torque sensor is developed in this section for the collision detection. The torque sensor material composition is determined by analysis and comparison. Strain gauge torque sensors have two types of structural diagrams 1) Spoke structure and 2) Shear structure. These types are distinguished based on the strain gauge position and the flexure structure. In this article, the spoke structure type sensor is selected based on the sensor thickness and sensitivity. To receive the signal using the Wheatstone bridge unit, the number of spokes is kept to 4. To obtain high sensitivity during the dynamic load torque, stress must be concentrated on the spoke region. Besides, the tension must be uniformly distributed during the dynamic load torque to obtain a smooth output voltage signal.

The disadvantage of non-perforated spoke structure is the concentration of high-stresses produces near the interior hub as shown in Figure 1a. Although, it is very problematic to glue the strain gauges near the interior hub due to short space. The strain gauges should be glued on the high- stress region to effectively measure the dynamic torque. To resolve this issue, the sensor structure is modified so that the high-stress region shift to the center part of the spoke radius as well as allows to paste the strain gauges easily on to the high-stress area. Figure 1b shows the modified perforated spoke structure and Figure 2 shows its dimensions.

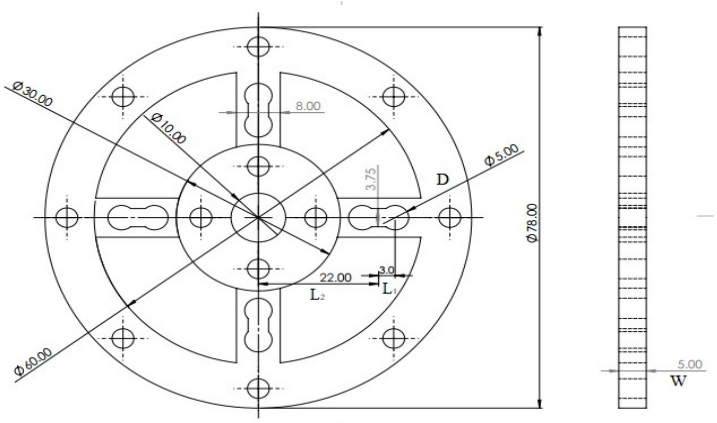

Figure 2: Perforated spoke type torque sensor dimensions.

The procedure for the material selection is to finalize that the sensor must have enough capacity to bear the deformation over extreme load. Frequently, the fourth theory of force is utilized to verify the strength of the structure to keep the spoke structure in the safe region for the given loads (Zhenlin et al., 2003).

$$\sigma_{1V} \leq [\sigma] = \frac{\sigma_s}{n_s C_{ol}} \quad (1)$$

where σ_{1V} represents the Von Mises equivalent stress which can be calculated by the Finite Element Analysis (FEA) simulation. While σ_{1V}, n_s, and C_{ol} represent the yield force, the factor of safety, and overload capacity respectively. Three commonly used mechanical materials 1045 steel, 6061 aluminum alloy, and 7075 aluminum alloy were examined using FEA simulation for torque sensor fabrication. Table 2 presents the material properties.

Table 2: Material Properties

Material Property	7075 (SN)	6061 (SS)	AISI 1045
Max. allowable strain (MPa)	505	275	530
Admissible stress (MPa)	446.8	446.4	449.4
Max. strain (10^{-6})	3981	4153	1364

3.0 Structure Optimization

In previous section, we chose the initial dimensions of the torque sensor which may not be the optimized values. To get high sensitivity, compact structure, and capacity to handle maximum load, the proposed structure is optimized by using the topology optimization method. As per the working principle of the joint torque sensor, the outer hub is attached to the gearbox while inner hub is attached to the robot's link. When the robot's joint active, the outer hub produces rotational effect on the inner hub creates the stresses on each spoke. Figure 4 shows the strain gauges location S_1, S_2, S_3 and S_4. The strain gauges produce a torque signal depend on the load capacity followed by a necessary signal processing. From the working principle, it is concluded that the spoke structure can be replaced with the cantilever beam for the parameter optimization.

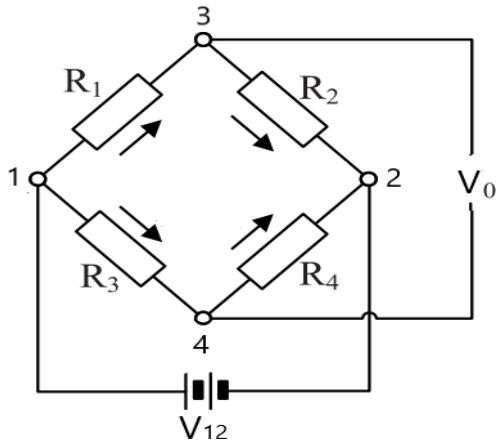

Figure 3: Wheatstone bridge

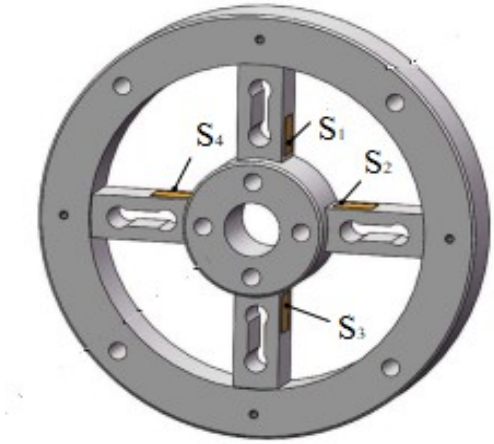

Figure 4: Location of strain gauges

Problem Formulation

The objective function $f(x)$ defines the relationship between the desired and the actual design variables. Normally, one objective function is enough for optimization of the joint torque sensor. To obtain the high performance, two objective functions are considered 1) Sensitivity $f_1(x)$ and 2) Strain gauge $f_2(x)$. Figure 3 shows the schematic of Wheatstone bridge. Where R_1, R_2, R_3 and R_4 represents bridge resistors while V_{12} and V_0 depicts voltage across terminals. The full voltage across terminal 3 and 4 can be written as

$$V_0 = V_{34} = V_{13} - V_{14} = \frac{R_1R_4 - R_2R_3}{(R_1+R_2)(R_3+R_4)}V_{12} \qquad (2)$$

Normally, all four resistors have same value and collectively represent by R. Under load condition, the strain gauges resistance varied according to the following relationship.

$$\frac{dR}{R} = \frac{d\rho}{\rho} + \frac{dL}{L} - \frac{dS}{S} = \frac{d\rho}{\rho} + (1+2v)\varepsilon = k_s \cdot \varepsilon \qquad (3)$$

where ρ, L, S, ks, and ε represents the metal wire resistivity, wire length, wire cross-sectional area, metal wire sensitivity and average strain, respectively. By small change in each resistor, the bridge voltage can be written as

$$V_0 = \frac{(R + \Delta R_1)(R + \Delta R_2) - (R + \Delta R_3)(R + \Delta R_4)}{(2R + \Delta R_1 + \Delta R_2)(2R + \Delta R_3 + \Delta R_4)} V_{12}$$

$$V_0 = \frac{V_{12}}{4} K_1(\varepsilon_1 - \varepsilon_2 - \varepsilon_3 + \varepsilon_4) \quad (4)$$

where K1 depicts strain gauge sensitivity and ei represent the average strain along the axial path. The sensor sensitivity K can be expressed as

$$'K = \frac{V_{12}}{4} K_1 f_1(x) \quad (5)$$

where,

$$f_1(x) = \frac{(\varepsilon_{21} - \varepsilon_{22} - \varepsilon_{23} + \varepsilon_{24}) - (\varepsilon_{11} - \varepsilon_{12} - \varepsilon_{13} + \varepsilon_{14})}{T_2 - T_1}$$

The term e1,i, i = 1, . . . , 4 represents the ith strain gauge value for input T1 while e2,j , j = 1, . . . , 4 depicts with T2 input. The sensitivity f1(x) function should be maximized for higher sensitivity. The objective function for the invariability of stresses produced at spoke can be expressed by the maximum difference between the strain values.

$$f_2(x) = \varepsilon_{max} - \varepsilon_{min} \quad (6)$$

To achieve the desired strength, the sensor must satisfy the fourth strength theory under 250% overload capacity. The optimization constraints are.

$$n_s \rightarrow 1^+$$
$$x - x_{max} \leq 0$$
$$x_{min} - x \leq 0$$

The complete optimization problem is expressed as follows.

$$max f_1(x)$$
$$min f_2(x)$$
$$s.t\ n_s \rightarrow 1^+$$
$$x - x_{max} \leq 0$$
$$x_{min} - x \leq 0$$
$$x = [D, L_1, L_2, W]^T \in R^4$$

4.0 Simulations and Results

To analyze the performance of the spoke structure type torque sensor, two models are presented as shown in Figure 1. Figure 2 shows the initial guesses of the parameters that are selected based on the designer experience. The FEA is performed using SolidWorks by applying the torque at an internal hub and keeping the external hub fixed. Figure 5 shows the corresponding stresses values for both the structures. It is observed that the spoke structure with a hole has high stresses as compared to non-perforated spoke structure. Table 3 presents the FEA analysis of different materials. Hence, the stress of the perforated spoke is further intense as compared to non-perforated spoke.

The high-stress region is shifted from the interior hub to the center of the spoke to facilitate the pasting of the strain gauges on the high-stress area. In addition, the linearity of the sensor is further improved due to the uniform distribution of the stresses. The maximum constant load torque is kept 75 Nm. The analysis is performed on perforated spoke structure as well as on non-perforated spoke structure. It can be observed that 1045 steel and 7075 aluminum alloy have high stresses as expressed in Table 3. It is also observed that the 7075 aluminum alloy has better strain as compared to 1045 steel, which provides high sensitivity. In addition, the density of 7075 aluminum

alloy is smaller, resulted in a light-weight senor.

The design parameters D, L1, L2, and W are considered for the optimization as shown in Figure 2 due to its dependency on the sensor functionalities. The rest of the structure dimensions are kept constant during the optimization process. Table 4 presents the upper and lower bounds of design variables. For the given design parameters, the SolidWorks was used for topology optimization. The optimal values are presented in Table 5. The torque sensor thickness is condensed by 35% while sensitivity is improved by 45.5%. The ns rate is reduced to 1.08. Overall, the torque sensor performance is greatly improved by topology optimization.

5.0 Discussion

From the assessment of both type torque sensors, it can be observed that the proposed joint torque sensor justified the design constraints properly. To achieve the improved sensitivity, fast response, and a compact shape, the aluminum alloy 7075 was selected among the multiple specimens with 75 g mass and 9 mm thickness. As well as it can be easily integrated with the robot's joint. For the real-time application, the sensor resolution and response frequency are kept constant to 0.1 Nm and 2 kHz, respectively. The torque sensor thickness is significantly reduced. The factor of safety is reduced to ensure lightweight construction of torque sensor. Overall, the torque sensor performance is greatly improved by topology optimization.

Table 3: Simulation Results

Material types		7075-T6 (SN)				6061-T6 (SS)				AISI 1045 Steel			
Spoke types	Type	With Slot		Without Slot		With Slot		Without Slot		With Slot		Without Slot	
Para.		Min	Max	Min	Max	Min	Max	Min	Max	Min	Max	Min	Max
Stress (N/m^2)	VMS	4.12×10^4	4.79×10^8	4.92×10^5	2.08×10^8	1.85×10^4	2.15×10^8	4.11×10^5	1.73×10^8	1.85×10^4	2.15×10^8	6.40×10^5	3.17×10^8
Displ. (mm)	URES	0	0.1456	0	0.0447	0	0.0680	0	0.0380	0	0.0690	0	0.0230
Strain	ESTRN	5.9×10^{-7}	3.9×10^{-3}	1.48×10^{-5}	2.42×10^{-3}	2.75×10^{-7}	1.83×10^{-3}	1.29×10^{-5}	2.11×10^{-3}	2.75×10^{-7}	1.83×10^{-3}	7.20×10^{-6}	1.2×10^{-3}
F.O.S	Auto	1.053	1.22×10^4	2.426	1.03×10^3	1.280	1.49×10^4	1.585	6.69×10^2	1.280	1.49×10^4	1.670	8.36×10^2

Table 4: Variables upper and lower limits

Variables	D (mm)	L_1 (mm)	L_2 (mm)	W (mm)
Upper bound	5	4	23	6
Lower bound	3	2	20	4

Table 5: Optimal Values

Variables	D (mm)	L_1 (mm)	L_2 (mm)	W (mm)	σ MPa	n_S
Initial Values	4.03	2.03	21.75	4.98	367.6	1.37
Optimal Values	4	2	21.5	4.2	452.3	1.11

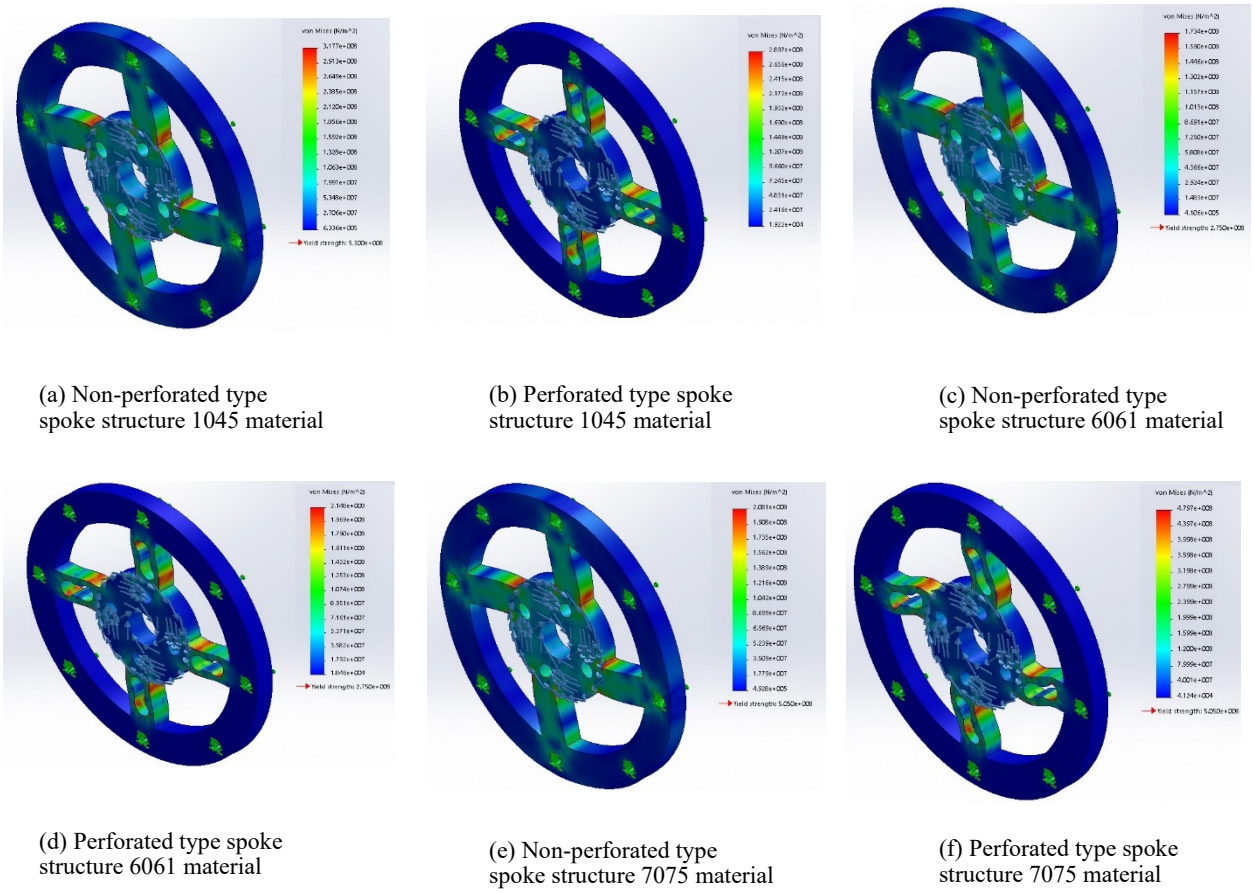

(a) Non-perforated type spoke structure 1045 material

(b) Perforated type spoke structure 1045 material

(c) Non-perforated type spoke structure 6061 material

(d) Perforated type spoke structure 6061 material

(e) Non-perforated type spoke structure 7075 material

(f) Perforated type spoke structure 7075 material

Figure 5: Stress analysis of spoke type joint torque sensor

6.0 Conclusion

In this study, we proposed the design and analysis of a joint torque sensor for a safe human-robotic collaboration. The perforated spoke structure is presented to ensure fast collision detection to avoid severe damage. The strain gauges locations are shifted to high-stress region in the middle of the spoke to obtain a smooth voltage signal. The comparison among the most used materials is performed by the Finite Element Analysis technique using the SolidWorks. The aluminum alloy 7075 is selected among the tested materials for improved sensitivity, light-weight, and high strength capability. By topology optimization, the torque sensor thickness was reduced by 29.97% and the n_s rate was reduced by 18.72%.

References:

F. Dimeas, V. C. Moulianitis, and N. Aspragathos, “Manipulator performance constraints in human-robot cooperation,” Robotics and Computer-Integrated Manufacturing, vol. 50, no. September, pp. 222–233, 2018. [Online]. Available: https://doi.org/10.1016/j.rcim.2017.09.015.

D. E. Choi, G. H. Yang, J. Choi, W. Lee, C. Cho, and S. Kang, “A safe joint with a joint torque sensor,” URAI 2011 - 2011 8th International Conference on Ubiquitous Robots and Ambient Intelligence, pp. 331–336, 2011.

S. Haddadin, A. De Luca, and A. Albu-Schäffer, “Robot collisions: A survey on detection, isolation, and identification,” IEEE Transactions on Robotics, vol. 33, no. 6, pp. 1292–1312, 2017.

D. Han, H. Nie, J. Chen, and M. Chen, “Dynamic obstacle avoidance for manipulators using distance calculation and discrete detection,” Robotics and Computer-Integrated Manufacturing, vol. 49, no. November 2016, pp. 98–104, 2018. [Online]. Available: http://dx.doi.org/10.1016/j.rcim.2017.05. 013.

S. D. Lee, M. C. Kim, and J. B. Song, “Sensorless collision detection for safe human-robot collaboration,” IEEE International Conference on Intelligent Robots and Systems, vol. 2015-Decem, pp. 2392–2397, 2015.

S. Chen, M. Luo, and F. He, "A universal algorithm for sensorless collision detection of robot actuator faults," Advances in Mechanical Engineering, vol. 10, no. 1, pp. 1–10, 2018.

B. Munoz-Barron, J. R. Rivera-Guillen, R. A. Osornio-Rios, and R. J. Romero-Troncoso, "Sensor Fusion for Joint Kinematic Estimation in Serial Robots Using Encoder, Accelerometer and Gyroscope," Journal of Intelligent and Robotic Systems: Theory and Applications, vol. 78, no. 3-4, pp. 529–540, 2015.

A. Mohammed, B. Schmidt, and L. Wang, "Active collision avoidance for human–robot collaboration driven by vision sensors," International Journal of Computer Integrated Manufacturing, vol. 30, no. 9, pp. 970–980, 2017. [Online]. Available: http://dx.doi.org/10.1080/0951192X.2016.1268269.

J. Kim, A. Alspach, and K. Yamane, "3D printed soft skin for safe human-robot interaction," IEEE International Conference on Intelligent Robots and Systems, vol. 2015-Decem, pp. 2419– 2425, 2015.

Y. Wang, G. Zuo, X. Chen, and L. Liu, "Strain Analysis of Six-Axis Force/Torque Sensors Based on Analytical Method," IEEE Sensors Journal, vol. 17, no. 14, pp. 4394–4404, 2017.

C. Park, H. M. Do, G. Jo-Jung, and B. I. Kim, "Performance test equipment design of a 1 DOF joint torque sensor," 2013 10th International Conference on Ubiquitous Robots and Ambient Intelligence, URAI 2013, pp. 674–676, 2013.

S. Y. Choi, T. K. Kim, D. Y. Kim, B. S. Kim, J. H. Hwang, and C. W. Park, "Development of joint torque sensor applied to compensate crosstalk error," IEEE International Conference on Automation Science and Engineering, pp. 1086–1088, 2012.

O. Al-Mai, M. Ahmadi, and J. Albert, "A Compliant 3-Axis Fiber-Optic Force Sensor for Biomechanical Measurement," IEEE Sensors Journal, vol. 17, no. 20, pp. 6549–6557, 2017.

G. Palli and S. Pirozzi, "An Optical Torque Sensor for Robotic Applications," International Journal of Optomechatronics, vol. 7, no. 4, pp. 263–282, 2013.

O. Al-Mai, M. Ahmadi, and J. Albert, "Design, Development and Calibration of a Lightweight, Compliant Six-Axis Optical Force/Torque Sensor," IEEE Sensors Journal, vol. 18, no. 17, pp. 7005–7014, 2018.

A. M. Madni, J. B. Vuong, D. C. Yang, and B. Huang, "A differential capacitive torque sensor with optimal kinematic linearity," IEEE Sensors Journal, vol. 7, no. 5, pp. 800–807, 2007.

D. H. Lee, U. Kim, H. Jung, and H. R. Choi, "A capacitive type novel six-axis force/torque sensor for robotic applications," IEEE Sensors Journal, vol. 16, no. 8, pp. 2290–2299, 2016.

J. Choi, S. Kim, J. Lee, and B. Choi, "Improved capacitive pressure sensors based on liquid alloy and silicone elastomer," IEEE Sensors Journal, vol. 15, no. 8, pp. 4180–4181, 2015.

S. Park, S. Y. Kim, and I. Kang, "Development of a spoke type novel joint torque sensor by using nano carbon strain sensors," 2014 11th International Conference on Ubiquitous Robots and Ambient Intelligence, URAI 2014, no. Urai, pp. 494–495, 2014.

Y. Sun, Y. Liu, M. Jin, and H. Liu, "Design of a novel six-axis force/torque sensor based on strain gauges by finite element method," Proceedings of the World Congress on Intelligent Control and Automation (WCICA), vol. 2015-March, no. March, pp. 3387–3392, 2015.

N. Kashiri, J. Malzahn, and N. G. Tsagarakis, "On the Sensor Design of Torque Controlled Actuators: A Comparison Study of Strain Gauge and Encoder-Based Principles," IEEE Robotics and Automation Letters, vol. 2, no. 2, pp. 1186–1194, 2017.

M. Hilal Muftah, M. Mohamed Haris, K. Petroczki, and E. Awad Khidir, "An improved strain gauge-based dynamic torque measurement method," International Journal of Circuits, Systems and Signal Processing, vol. 7, no. 1, pp. 66–73, 2013.

J. Missinne, A. Monté, Y. Tijtgat, N. Rossey, and G. Van Steenberge, "Miniature multiaxial optoelectronic shear stress sensing system based on a segmented photodiode," IEEE Sensors Journal, vol. 15, no. 8, pp. 4286–4291, 2015.

S. Lee, K. Yang, E. Shin, and H. Kim, "Development of 1-axis torque sensor with different shape of support and measurement spoke," 2014 11th International Conference on Ubiquitous Robots and Ambient Intelligence, URAI 2014, no. Urai, pp. 688–691, 2014.

K. Suita, Y. Yamada, N. Tsuchida, K. Imai, H. Ikeda, and N. Sugimoto, "Failure-to-safety 'Kyozon' system with simple contact detection and stop capabilities for safe humanautonomous robot coexistence," Proceedings - IEEE International Conference on Robotics and Automation, vol. 3, pp. 3089– 3096, 1995.

Y. Yamada, Y. Hirasawa, S. Huang, Y. Umetani, and K. Suita, "Human-robot contact in the safeguarding space," IEEE/ASME Transactions on Mechatronics, vol. 2, no. 4, pp. 230–236, 1997.

J. Zhenlin, G. Feng, and Z. Xiaohui, "Design and analysis of a novel isotropic six-component force/torque sensor," Sensors and Actuators, A: Physical, vol. 109, no. 1-2, pp. 17–20, 2003.

Biographies

Muhammad Bilal has completed his BSc in Mechatronics Engineering from UET Faisalabad and currently pursuing his MSc from Mechatronics and Control Engineering department UET Lahore. He has a deep interest in Human-Centered Robotics.

Sajid Iqbal did his PhD in Mechatronics Engineering from Harbin Institute of Technology (HIT), China. He received his BSc and MSc in Electrical Engineering from University of Engineering and Technology (UET) Lahore, where he is currently serving as an Assistant Professor in the Department of Mechatronics & Control Engineering. He was awarded *'Young Investigators Award'* at 2018 Sage Assembly and CICOPS (Centre for International Cooperation and Development) scholarship in 2019. He is an HEC approved PhD supervisor. His current research interests include nonlinear dynamics, chaos, electronic circuits, TRIZ, and education. He is a certified TRIZ Level-1 Instructor and Level-2 Practitioner from Malaysia.

Muhammad Nadeem Akram is a PhD student of Industrial and Manufacturing System Engineering in the Department of Mechanical, Automotive, and Materials Engineering, Faculty of Engineering, University of Windsor, Windsor, Ontario, Canada. He earned his B.Sc. in Mathematics and Physics from the University of Punjab, Pakistan, his B.Sc. in Electrical Engineering from the University of Engineering and Technology, Pakistan, his Master of Industrial Engineering, and his Master of Applied Sciences in Industrial Engineering from the University of Windsor, Windsor, Ontario, Canada. His research interests include sustainable manufacturing, Electric Vehicles and Batteries of Electric Vehicles.